

© 2022 IEEE. Personal use of this material is permitted. Permission from IEEE must be obtained for all other uses, including reprinting/republishing this material for advertising or promotional purposes, collecting new collected works for resale or redistribution to servers or lists, or reuse of any copyrighted component of this work in other works. This work has been submitted to the IEEE for possible publication. Copyright may be transferred without notice, after which this version may no longer be accessible.

Nonlinear Subsystem-based Adaptive Impedance Control of Physical Human-Robot-Environment Interaction in Contact-rich Tasks

Mahdi Hejrati , Jouni Mattila , Member, IEEE

Abstract—Haptic upper limb exoskeletons are robots that assist human operators during task execution while having the ability to render virtual or remote environments. Therefore, the stability of such robots in physical human-robot-environment interaction must be guaranteed, in addition to performing well during task execution. Having a wide range of Z-width, which shows the region of passively renderable impedance by a haptic display, is also important to render a wide range of virtual environments. To address these issues, in this study, subsystem-based adaptive impedance control is designed for having a stable human-robot-environment interaction of 7 degrees of freedom haptic exoskeleton. The presented control decomposes the entire system into subsystems and designs the controller at the subsystem level. The stability of the controller in the presence of contact with the virtual environment and human arm force is proved by employing the virtual stability concept. Additionally, the Z-width of the 7-DoF haptic exoskeleton is drawn using experimental data and improved using varying virtual mass element for the virtual environment. Finally, experimental results are provided to demonstrate the perfect performance of the proposed controller in accomplishing the predefined task.

Index Terms—Adaptive impedance control, physical human-robot-environment interaction, haptic exoskeleton

I. INTRODUCTION

WITH advancements in technology related to the Fourth Industrial Revolution, robots are increasingly being utilized in industries to reduce the workload of workers and in healthcare to improve the quality of human life, showing the significance of human-robot interaction (HRI). HRI can be divided into three categories of human-robot coexistence, human-robot cooperation, and human-robot collaboration or physical HRI (pHRI) [1]. Unlike to first two categories, in the pHRI scenario, the human and robot are working together on the same task while having a physical impact on each other. An upper limb exoskeleton (ULE) is one example of such an interaction [2]. On the other hand, a haptic ULE (HULE) [3] incorporates haptic display technology to render a virtual or remote environment along with the ULE assistance feature. HULE can either be utilized as a master robot in bilateral

The TITAN (Teaching human-like abilities to heavy mobile manipulators through multisensory presence) project is funded by the Technology Industries of Finland Centennial Foundation and the Jane and Aatos Erkko Foundation Future Makers programme. 2020-2023.

M. Hejrati, corresponding author, is with the Department of Engineering and Natural Science, Tampere University, 7320 Tampere, Finland (e-mail: mahdi.hejrati@tuni.fi).

J. Mattila is with the Department of Engineering and Natural Science, Tampere University, 7320 Tampere, Finland (e-mail: Jouni.Mattila@tuni.fi).



Fig. 1. Physical human-robot-environment interaction of haptic upper limb exoskeleton (HULE), a) as a master robot in bilateral teleoperation for rendering remote environment b) as an assisting device for co-manipulation

teleoperation control with the ability to render a remote environment or assist a human during contact-rich co-manipulation (Fig. 1). Consequently, HULE is impacted by human upper limb dynamics along with contact with the virtual or physical environments. Therefore, it is crucial to ensure the stability of physical human-robot-environment interaction (pHREI) in HULE while contact-rich tasks are executed. Physical human-robot-environment interaction control can be implemented by means of the impedance control scheme [4], which provides the robot a safe and robust compliant behavior throughout interactions with humans and the environment. Additionally, for a haptic display, the Z-width is a key feature that represents the dynamic range of passive impedances that can be rendered. With a larger Z-width, HULE can render a larger range of virtual or remote environments with better feelings [5]. For this reason, Z-width is an important consideration for haptic display, and maximizing it is desirable.

II. RELATED WORKS

A. Impedance Control in pHRI

Throughout the pHREI, the goal of HULE is to accomplish the task (which can be co-manipulation or assistance) despite the impact of human upper limb dynamics and contact with the environment. Impedance control, which has been widely utilized in the field of robotics [6], [7], can equip HULE with such an ability. A multi-point impedance control has been designed to control the pHREI of a 2-DoF robot in [8]. In [9], an adaptive impedance control has been designed to control ULE, in which the impedance parameters of the controller are tuned using surface electromyography and the musculoskeletal model of the human upper limb. In [10], an adaptive impedance control has been designed for ULE control based on the muscle circumference sensor for human intention estimation. The goal of that study is to assist a

human while carrying an object by using 7-Dof ULE with 5 passive and 2 active DoFs. Adaptive backstepping impedance control is proposed in [11] for rehabilitation applications using 7-DoF ULE. Moreover, in [12] iterative learning impedance control has been proposed to control a 1-DoF ULE driven by series elastic actuators, and the desired impedance has been achieved through the iterative manner of the controller. Impedance control has been utilized to control the haptic display as well. In [13], nonlinear model reference adaptive impedance control has been proposed to control 5-DoF haptic display. Weighted admittance-impedance control is designed for pHREI control of a 2-DoF haptic device in [14]. All the mentioned works examined either ULE or haptic devices with low DoFs, whereas, in this study, HULE is a 7-DoF wearable haptic display (Fig. 1). Therefore, it is crucial to ensure the stability and performance of the controller in the presence of human and environmental impact along with considering the complexity of the system, which guarantees human safety inside HULE.

B. Z-width

Generally, an environment can be represented by a second-order mass-spring-damper impedance model,

$$Z(s) = Ms + B + \frac{K}{s} \quad (1)$$

with M, B, and K being the mass, damping, and stiffness coefficients of the environment, respectively. As virtual wall enables us to examine the haptic display and impedance control performance in both high-impedance (having contact with a virtual wall) and low-impedance (free motion) scenarios, in this study, we considered the environment as a unilateral constraint (wall). A larger Z-width means that the haptic display can render a virtual wall with a wider range of stiffness. Therefore, it is important to have a larger Z-width in HULE. Numerous studies have attempted to enhance the Z-width of a haptic display by examining various issues. In [15], [16], the effect of an increase in sampling rate has been analyzed. A dual-rate sampling method is proposed in [17]. However, adding virtual coupling to haptic devices has been a significant approach to increasing the range of the Z-width, as introduced in [18]. In several works, virtual damping has been proposed to enhance the Z-width [19], [20]. Nevertheless, in [21], it has been shown that using virtual inertia can expand the Z-width of a 1-Dof haptic device more than when virtual damping is employed. All previous works analyzed the Z-width for unwearable low-DoF haptic devices only for performance analysis. By contrast, for high-DoF nonlinear haptic exoskeletons (Fig. 1), it must be ensured that the achieved Z-width is passive in the presence of human effects and extracted for real-world applications.

C. Aims and Contributions

Based on the literature overview, the aim of the present study is to develop a high-performance HULE with stable interactions with the virtual environment in the presence of human arm dynamics. The contributions of this paper are as

follows. First, a subsystem-based adaptive impedance scheme is designed to control the end-effector pose of 7-DoF HULE in the contact-rich task. The proposed controller decomposes the entire system into subsystems, which enables us to design a controller without dealing with non-linearities at the subsystem level. Instead, the non-linearities of the entire system along with the human arm forces and contact with the environment are considered in the overall control law. The natural adaptation law (NAL) is incorporated into the controller to estimate the unknown parameters of the HULE by requiring only one adaptation gain [22]. NAL also ensures the physical consistency condition for the estimated parameters. The results are validated by performing experiments. Second, the Z-width of HULE is experimentally drawn in the presence of human arm dynamics and impedance controller by considering all the nonlinearities of the 7-DoF HULE, which makes the derived achievable Z-width much more reliable in a real-world application. Additionally, the varying virtual mass element is employed as a new damping element to enhance the Z-width of HULE.

The paper is organized as follows. In Section III, the mathematical foundation of the approach is described, and the problem is formulated. In Section IV, the proposed subsystem-based impedance control is presented, and in Section V, details of Z-width improvement are given. The experimental results are provided in Section VI with the conclusion part in Section VII.

III. SUBSYSTEM-BASED CONTROL SCHEME

A. Virtual Decomposition Control

Virtual decomposition control (VDC) [23] is a model-based control approach that is suitable for highly nonlinear systems. To design the control action, VDC decomposes the complex robotic system into the actuator and rigid body subsystems using the virtual cutting point (VCP) concept (Fig. 3). Additionally, it distributes the control objective of the entire system to the local control objectives of subsystems. Then, it computes the required forces and torques, which are required to accomplish local control goals, based on the Newton-Euler iterative method for a given required velocity. Required velocity is the design variable in VDC and must be designed based on the given task. The stability of each subsystem is proved at the local subsystem level and expanded to the stability of the entire complex system by employing a scalar term called the virtual power flow (VPF) and virtual stability scheme. Thereby, this method is specifically designed for controlling complex systems, such as pHREI control of a 7-DoF HULE. The VDC scheme has shown great performance in various fields, such as teleoperation [24], impedance control of hydraulic manipulators [25], and ULE control [22]. In this paper, a modified version of the VDC approach [22] is employed.

B. VDC Mathematical Preliminaries

Definition 1. [23] For a given frame $\{B_i\}$ at the VCP, the VPF is defined as,

$$p_{B_i} = ({}^{B_i}\mathcal{V}_r - {}^{B_i}\mathcal{V})^T ({}^{B_i}\mathcal{F}_r - {}^{B_i}\mathcal{F}). \quad (2)$$

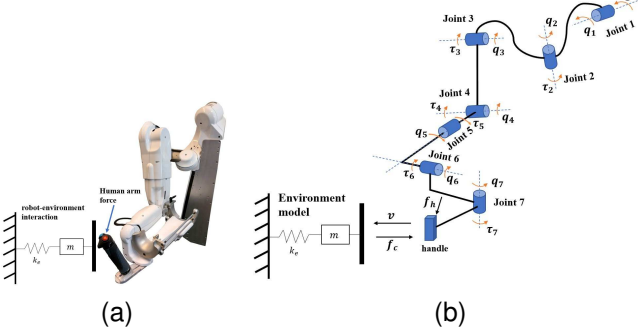


Fig. 2. a) HULE in contact with a virtual wall, b) joint configuration

Definition 2. [23] A subsystem that is virtually decomposed from a complex robot is said to be virtually stable with its affiliated vectors $\mathcal{X}(t)$ and $y(t)$ being a virtual function, if and only if there exists a non-negative accompanying function

$$\nu(t) \geq \frac{1}{2} \mathcal{X}(t)^T P \mathcal{X}(t) \quad (3)$$

such that,

$$\dot{\nu}(t) \leq -y(t)^T Q y(t) + p_A - p_C \quad (4)$$

where P and Q are two block-diagonal positive-definite matrices, and p_A and p_C denote VPFs in the sense of Definition 1 at frames $\{\text{A}\}$ (placed at the driven VCPs) and $\{\text{C}\}$ (placed at the driving VCPs).

Theorem 1. [23] Consider a complex robot that is virtually decomposed into subsystems. If all the decomposed subsystems are virtually stable in the sense of Definition 1, then the entire system is stable.

Theorem 1 is the most important theorem in the VDC context. It establishes the equivalence between the virtual stability of every subsystem and the stability of the entire complex robot.

Lemma 1. [22] For any inertial parameter vector ϕ , there is a one-to-one linear map $f : \mathbb{R}^{10} \rightarrow S(4)$ such that,

$$f(\phi) = \mathcal{L} = \begin{bmatrix} 0.5\text{tr}(\bar{I}) \cdot \mathbf{1} - \bar{I} & h \\ h^T & m \end{bmatrix}$$

$$f^{-1}(\phi) = \phi(m, h, \text{tr}(\Sigma) \cdot \mathbf{1} - \Sigma_B)$$

where $\Sigma_B = 0.5\text{tr}(\bar{I}_B) - \bar{I}_B$, and m, h , and \bar{I} are the mass, first mass moment, and rotational inertia matrix, respectively. Moreover, $\text{tr}(\cdot)$ is the Trace operator of a matrix.

Lemma 2. [22] For \mathcal{L} defined in Lemma 1, Bregman divergence with the log-det function can be defined as,

$$\mathcal{D}_F(\mathcal{L} \parallel \hat{\mathcal{L}}) = \log \frac{|\hat{\mathcal{L}}|}{|\mathcal{L}|} + \text{tr}(\hat{\mathcal{L}}^{-1} \mathcal{L}) - 4.$$

with the time derivative of,

$$\dot{\mathcal{D}}_F(\mathcal{L} \parallel \hat{\mathcal{L}}) = \text{tr}([\hat{\mathcal{L}}^{-1} \dot{\hat{\mathcal{L}}} \hat{\mathcal{L}}^{-1}] \tilde{\mathcal{L}})$$

where $\tilde{\mathcal{L}} = \hat{\mathcal{L}} - \mathcal{L}$.

C. VDC Control Design

Consider $\{B_i\}$ and $\{T_i\}$ as frames that are attached to the i^{th} rigid body. Then, the 6D linear/angular velocity vector ${}^{B_i}\mathcal{V} \in \mathbb{R}^6$ and force/moment vector ${}^{B_i}\mathcal{F} \in \mathbb{R}^6$ can be expressed as follows [23]:

$${}^{B_i}\mathcal{V} = [{}^{B_i}v, {}^{B_i}\omega]^T, \quad {}^{B_i}\mathcal{F} = [{}^{B_i}f, {}^{B_i}m]^T$$

where ${}^{B_i}v \in \mathbb{R}^3$ and ${}^{B_i}\omega \in \mathbb{R}^3$ are the linear and angular velocities of frame $\{B_i\}$, and ${}^{B_i}f \in \mathbb{R}^3$ and ${}^{B_i}m \in \mathbb{R}^3$ are the force and moment expressed in frame $\{B_i\}$, respectively. The transformation matrix that transforms force/moment vectors and velocity vectors between frames $\{B_i\}$ and $\{T_i\}$ is [23],

$${}^{B_i}U_{T_i} = \begin{bmatrix} {}^{B_i}R_{T_i} & \mathbf{0}_{3 \times 3} \\ ({}^{B_i}r_{B_i T_i} \times) {}^{B_i}R_{T_i} & {}^{B_i}R_{T_i} \end{bmatrix} \quad (5)$$

where ${}^{B_i}R_{T_i} \in \mathbb{R}^{3 \times 3}$ is a rotation matrix between frame $\{B_i\}$ and $\{T_i\}$, and $({}^{B_i}r_{B_i T_i} \times)$ is a skew-symmetric matrix operator defined in [23]. Based on ${}^{B_i}U_{T_i}$, the force/moment and velocity vectors can be transformed between frames as [23],

$${}^{T_i}\mathcal{V} = {}^{B_i}U_{T_i}^T {}^{B_i}\mathcal{V}, \quad i = 1 \dots 7 \quad (6)$$

$${}^{B_i}\mathcal{V} = \kappa_i \dot{q}_i + {}^{T_{i-1}}U_{B_i}^T {}^{T_{i-1}}\mathcal{V}, \quad i = 1 \dots 7 \quad (7)$$

$${}^{B_i}\mathcal{F} = {}^{B_i}F^* + {}^{B_i}U_{T_i} {}^{T_i}F, \quad i = 7 \dots 1 \quad (8)$$

with ${}^{T_{i-1}}F = {}^{T_{i-1}}U_{B_i} {}^{B_i}F$ for $i = 7 \dots 1$, q_i and \dot{q}_i being joint angles and velocities, respectively, $\kappa_i = z_\tau$ for $i = 1, 2, 3, 4, 6$, $\kappa_i = y_\tau$ for $i = 7$, and $\kappa_i = x_\tau$ for $i = 5$, which $z_\tau = [0, 0, 0, 0, 0, 1]^T$, $y_\tau = [0, 0, 0, 0, 1, 0]^T$, $x_\tau = [0, 0, 0, 1, 0, 0]^T$, and $(\cdot)^T$ is Transpose operator. Moreover, for $i = 1$ we have ${}^{T_0}\mathcal{V} = {}^G\mathcal{V} = \mathbf{0}_{6 \times 1}$ and ${}^{T_0}F = \mathbf{0}_{6 \times 1}$, and for $i = 7$, we have ${}^{T_7}F = f$, where f is the interaction force and will be defined later. ${}^{B_i}F^*$ is the net force applied to the i^{th} rigid body, defined as,

$$M_{B_i} \frac{d}{dt} ({}^{B_i}\mathcal{V}) + C_{B_i} ({}^{B_i}\mathcal{V}) + G_{B_i} = {}^{B_i}F^* \quad (9)$$

where $M_{B_i} \in \mathbb{R}^{6 \times 6}$, $C_{B_i} \in \mathbb{R}^{6 \times 6}$, and $G_{B_i} \in \mathbb{R}^6$ are the mass, centrifugal and Coriolis, and gravity matrices defined in [22], respectively. The local control objective for the rigid body part is to reach the given required linear/angular velocity ${}^{B_i}\mathcal{V}_r$, which will be defined later. Therefore, the required force/moment vector that must be applied to the i^{th} rigid body to accomplish local control objectives, can be designed as,

$${}^{B_i}F_r = {}^{B_i}F_r^* + {}^{B_i}U_{T_i} {}^{T_i}F_r. \quad (10)$$

with the local control law of,

$${}^{B_i}F_r^* = {}^{B_i}W \hat{\phi}_{B_i} + K_{Di} {}^{B_i}e_{\mathcal{V}} + K_{Ii} \int_0^t {}^{B_i}e_{\mathcal{V}} dt \quad (11)$$

where ${}^{B_i}e_{\mathcal{V}} = {}^{B_i}\mathcal{V}_r - {}^{B_i}\mathcal{V}$, and K_{Di} and K_{Ii} are diagonal positive-definite control gains, ${}^{B_i}W \in \mathbb{R}^{6 \times 10}$ is the regression matrix, and $\hat{\phi}_{B_i} \in \mathbb{R}^{10}$ is the estimation of inertial parameter vector $\phi_{B_i} \in \mathbb{R}^{10}$ [22] defined as,

$${}^{B_i}W \phi_{B_i} = M_{B_i} \frac{d}{dt} ({}^{B_i}\mathcal{V}_r) + C_{B_i} ({}^{B_i}\mathcal{V}_r) + G_{B_i} \quad (12)$$

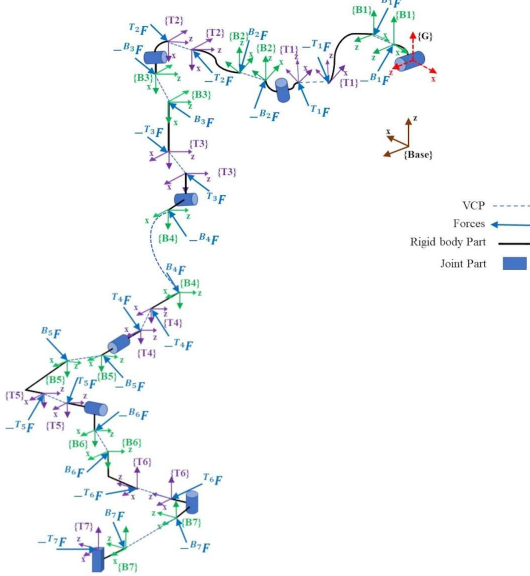


Fig. 3. Decomposition of 7 DoF HULE into subsystems of actuator and rigid body dynamics

The joint actuator dynamics for an electrical motor in the absence of friction can be expressed as,

$$I_{mi}\ddot{q}_i = \tau_i^* = \tau_i - \tau_{ai} \quad (13)$$

where I_{mi} denotes the moment of inertia of the joint. The equation (13) is exactly in the same sense as (10), with τ_i^* being the net torque applied to the joint, τ_i representing the control torque, and $\tau_{ai} = z^T B_i F$. It is obvious from (13) that the required torque for the actuator part, in order to achieve the local control objective, should first be able to compensate for rigid body dynamics and then control the joint angle. Therefore, the adaptive VDC control law for accomplishing both local control objectives can be designed as,

$$\tau_i = \tau_{ir}^* + \tau_{air} \quad (14)$$

with τ_{ir}^* being the local control law that ensures tracking of the desired angle for the joint, defined as,

$$\tau_{ir}^* = W_{ai}\hat{\phi}_{ai} + k_{di}e_{ai} + k_{Ii}\int_0^t e_{ai} \quad (15)$$

where $W_{ai} \in \mathbb{R}^{1 \times 10}$ is the regression matrix, and $\hat{\phi}_{ai} \in \mathbb{R}^{10}$ is the estimation of inertial parameter vector $\phi_{ai} \in \mathbb{R}^{10}$ in,

$$W_{ai}\phi_{ai} = I_{mi}\ddot{q}_i. \quad (16)$$

$e_{ai} = \dot{q}_{ir} - \dot{q}_i$ is the required angular velocity, k_{di} and k_{Ii} are positive control gains. Moreover, $\tau_{air} = z^T B_i F_r$ stands for accomplishing the local control objectives of a rigid body part with $B_i F_r$ being computed from (10). The estimation of inertial parameter vector in (11) and (15), denoted as $\hat{\phi}_{Bi}$ and $\hat{\phi}_{ai}$, can be computed by exploiting NAL [22],

$$\dot{\hat{\mathcal{L}}}_{Bi} = \frac{1}{\gamma} \hat{\mathcal{L}}_{Bi} \mathcal{S}_{Bi} \hat{\mathcal{L}}_{Bi} \quad (17)$$

$$\dot{\hat{\mathcal{L}}}_{ai} = \frac{1}{\gamma} \hat{\mathcal{L}}_{ai} \mathcal{S}_{ai} \hat{\mathcal{L}}_{ai} \quad (18)$$

where \mathcal{L}_{Bi} and \mathcal{L}_{ai} are pseudo inertia matrices corresponding to ϕ_{Bi} and ϕ_{ai} , respectively, defined in Lemma 1, with $\hat{\mathcal{L}}_{Bi}$ and $\hat{\mathcal{L}}_{ai}$ being the estimation of \mathcal{L}_{Bi} and \mathcal{L}_{ai} , respectively. \mathcal{S}_i is a unique symmetric matrix, and γ is the adaptation gain. As can be seen from (17) and (18), only one gain is required to be tuned for the estimation of unknown parameters of the HULE. Moreover, the only condition to satisfy the physical consistency condition of estimated parameters is that $\hat{\mathcal{L}}(0)$ be physically consistent [22].

The required linear/angular velocity, $B_i \mathcal{V}_r$, can be computed as,

$$B_i \mathcal{V}_r = \kappa_i \dot{q}_{ri} + T_{i-1} U_{B_i}^T T_{i-1} \mathcal{V}_r, \quad i = 1 \dots 7 \quad (19)$$

where $T_{i-1} \mathcal{V}_r$ is the required velocity of the VCP on the $(i-1)^{th}$ rigid body (for $i = 1$, we have, $T_0 \mathcal{V}_r = {}^G \mathcal{V}_r = \mathbf{0}_{6 \times 1}$), and \dot{q}_{ri} is the design variable and should be designed based on the predefined task. According to (19), if $\dot{q}_i \rightarrow \dot{q}_{ir}$, then $B_i \mathcal{V} \rightarrow B_i \mathcal{V}_r$, satisfying both local control objectives. The control law in (14) is designed in such a way that both parts are handled. Based on what is explained so far, the most important part of deriving VDC control law (14) is designing \dot{q}_{ir} . In this paper, in which the task space problem of a 7-DoF HULE is of concern, \dot{q}_{ri} can be defined as,

$$\dot{q}_{ri} = J^\dagger \dot{X}_r \quad (20)$$

with \dot{X}_r being the task space design variable, which will be defined later in a way to equip the robot with the desired impedance model, and

$$J^\dagger = J^T (J J^T)^{-1} \quad (21)$$

where $J \in \mathbb{R}^{6 \times 7}$ is the Jacobian matrix. In the next section, \dot{X}_r is designed in order to achieve the impedance control goal.

IV. IMPEDANCE CONTROL DESIGN

Impedance control equips the robot with the ability to accomplish both free-motion and contact-rich tasks. In free-motion tasks, it shows good performance in following the desired path, while in contact-rich tasks it can tolerate various environments. The desired impedance model for the robot can be expressed as [4],

$$-M_d(\ddot{X}_d - \ddot{X}) - B_d(\dot{X}_d - \dot{X}) - K_d(X_d - X) = f_d - f \quad (22)$$

where $M_d \in \mathbb{R}^{6 \times 6}$, $B_d \in \mathbb{R}^{6 \times 6}$, and $K_d \in \mathbb{R}^{6 \times 6}$, are diagonal positive-definite matrices and characterize the desired inertia, damping, and stiffness, respectively. f is the force applied to the HULE from the outside, and $e = X_d - X = [e_p, e_o]$, where e_p is the position error and e_o is orientation error using the quaternion [22] of the end-effector. As a haptic exoskeleton, HULE is impacted by human arm force f_h during the execution of the task and virtual environment force f_c whenever contact happens. Therefore, the external force applied to the robot during pHREI is different and can be expressed as,

$$f = \begin{cases} -f_h & : \text{assisting(pHRI)} \\ -f_h + f_c & : \text{contact(pHREI)} \end{cases} \quad (23)$$

The dynamic equation governing human arm dynamics can be expressed as,

$$M_h \ddot{X}_h + B_h \dot{X}_h + K_h (X_h - X) = f_h \quad (24)$$

where $M_h \in \mathbb{R}^{6 \times 6}$, $B_h \in \mathbb{R}^{6 \times 6}$, and $K_h \in \mathbb{R}^{6 \times 6}$, are diagonal positive-definite matrices and characterize the inertia, damping, and stiffness, matrices of the human arm, respectively, and X_h is human hand position. It must be mentioned that human exogenous force is omitted. The contact force f_c will be defined later. By neglecting the inertia in (22), the target impedance can be rewritten as,

$$-B_d(\dot{X}_d - \dot{X}) - K_d(X_d - X) = f_d - f. \quad (25)$$

The desired damping and stiffness should be selected in a way that is achievable by the robot without resulting in unstable behavior.

As mentioned previously, the required task space velocity in (20) is the control design variable for accomplishing desired objectives. The following theorem summarizes the subsystem-based impedance control law.

Theorem 2. For a decomposed system represented in (9) and (13) with the interaction force of (23), the desired impedance model (25) can be achieved for the robot if the design variable in (20), defined as,

$$\dot{X}_r = \dot{X}_d + \Gamma_x(X_d - X) + \Gamma_f(f_d - f) \quad (26)$$

with $\Gamma_x \in \mathbb{R}^{6 \times 6}$, and $\Gamma_f \in \mathbb{R}^{6 \times 6}$ being positive-definite diagonal matrices defined as,

$$\Gamma_f = B_d^{-1}, \quad \Gamma_x = K_d B_d^{-1}. \quad (27)$$

It must be mentioned that B_d and K_d should be selected from the achievable dynamic range of robot.

Proof. Appendix A.

The following theorem ensures the stability of the entire system in the sense of Theorem 1 and Definition 2.

Theorem 3. For a decomposed 7-DoF HULE (Fig. 3) with a rigid body and actuator dynamics of (9) and (13), control action of (14), adaptation laws of (17) and (18), and \dot{X}_r defined in (26), the non-negative accompanying function can be defined as,

$$\begin{aligned} \nu_i(t) = & \sum_{i=1}^7 \left[\frac{1}{2} \left(\int_0^t {}^{B_i} e \nu dt \right)^T K_{Ii} \left(\int_0^t {}^{B_i} e \nu dt \right) \right. \\ & + \frac{1}{2} k_{Ii} \left(\int_0^t e_{ai} dt \right)^2 + \frac{1}{2} {}^{B_i} e_{\nu}^T M_{B_i} {}^{B_i} e_{\nu} + \frac{1}{2} I_{mi} e_{ai}^2 \\ & \left. + \gamma \mathcal{D}_F(\mathcal{L}_{B_i} \|\hat{\mathcal{L}}_{B_i}) + \mathcal{D}_F(\mathcal{L}_{ai} \|\hat{\mathcal{L}}_{ai}) \right] \end{aligned} \quad (28)$$

where $\mathcal{D}_F(\mathcal{L} \|\hat{\mathcal{L}})$ is defined in Lemma 2. Taken the time derivative of (28), we can obtain,

$$\dot{\nu}_i(t) = \sum_{i=1}^7 \left(- {}^{B_i} e_{\nu}^T K_{Di} {}^{B_i} e_{\nu} - k_{di} e_{ai}^2 \right). \quad (29)$$

where, according to Theorem 1 and Definition 2, the asymptotic stability of the entire system is proven.

Proof. Appendix B.

V. Z-WIDTH OF HULE

For a haptic display, the Z-width is an indicator of the range of stiffness of a virtual wall that can be passively rendered. The passivity condition for contact with the generated force of $f_c(t)$ and haptic end-effector velocity of $v(t)$ can be defined as,

$$E_c(t) = \int_0^t f_c(\sigma) v(\sigma) d\sigma \geq 0. \quad \forall t \geq 0 \quad (30)$$

For a stiff virtual wall, the spring force can be computed as,

$$f_s(t) = k_e(z_e - z) \quad (31)$$

where k_e is the rendered stiffness of the virtual wall, z_e is the position of virtual wall, and z is the position of HULE end-effector. As can be seen from (30), increasing the stiffness of the virtual wall generates larger contact forces, resulting in unstable contact. Therefore, it limits the region of the Z-width. One alternative to having a wider Z-width (being able to render a larger k_e passively) is to add energy dissipative terms to the virtual wall. To do so, we employed the varying virtual mass as the energy dissipative element. After the contact between HULE end-effector and the virtual environment, unlike virtual damping, varying virtual mass is activated whenever the absolute amount of kinetic energy in the environment increases. Then, it dissipates the amount of energy that is equivalent to acceleration. Based on the explanation, varying virtual mass can be defined as,

$$m_e = S(u)m_d \quad (32)$$

where m_e is the virtual mass felt in the contact direction, m_d is the desired virtual mass that must be rendered in order to dissipate energy within the stable contact range, $S(u)$ is an activation function defined as,

$$S(u) = \begin{cases} 1 & \text{if } a.v \geq 0, \\ 0 & \text{else} \end{cases} \quad (33)$$

where a and v are the acceleration and velocity of the HULE end-effector in the direction of contact. The damping force of virtual elements can be computed as,

$$f_{damp} = \begin{cases} m_e a & \text{for varying virtual mass} \\ b_e v & \text{for virtual damping} \end{cases} \quad (34)$$

with b_e being virtual damping coefficient. Finally, the contact force can be computed as,

$$f_c(t) = f_s(t) + f_{damp}(t) \quad (35)$$

In the results section, the generated energy with both designed varying virtual mass and virtual damping is experimentally demonstrated using (30), and their effect on contact stability is examined. It is shown that employing varying virtual mass in (32) helps to achieve a larger Z-width.

VI. RESULTS

In this section, experimental results are provided to examine the performance of designed subsystem-based adaptive impedance control. Moreover, the effect of varying virtual mass on Z-width enhancement is shown.

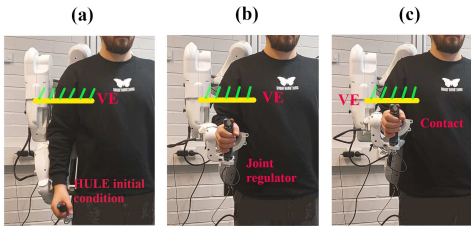


Fig. 4. Experiment steps for Z-width plot, a) initial configuration for HULE, b) VDC regulator calibrates joint angles, c) impedance control moves robot and contact happens. (VE: Virtual Environment)

A. Z-width Results

In this section, the Z-width of the HULE using both virtual damping and varying virtual mass is drawn. Fig. 4 demonstrates the experimental setup and steps for drawing Z-width. When the operator grasps the handle (Fig. 4(a)), HULE is activated at a random initial condition for joint angles. For a better comparison with having the same initial start point, a VDC-based joint regulator that moves HULE from an initial condition to a zero-angles configuration is employed (Fig. 4(b)). Then, to have the same contact condition, a 5th order smooth-acceleration trajectory generator is employed to generate a path between two given points in Cartesian space with the specified time t_f [26]. The lower t_f , the faster the trajectory and vice versa. Therefore, the start point and contact condition are set to be the same to examine the virtual damping and varying virtual mass effects on the Z-width. Finally, the proposed impedance control drives HULE from zero configuration to move in the z-direction of Cartesian space, where contact occurs (Fig. 4(c)). The desired impedance of the robot in (25) is fixed to $K_d = 100 \text{ diag}([2, 2, 1, 1, 1, 1]) \text{ N/m}$ and $B_d = 40 \text{ diag}([1, 1, 1, 1, 1, 1]) \text{ Ns/m}$.

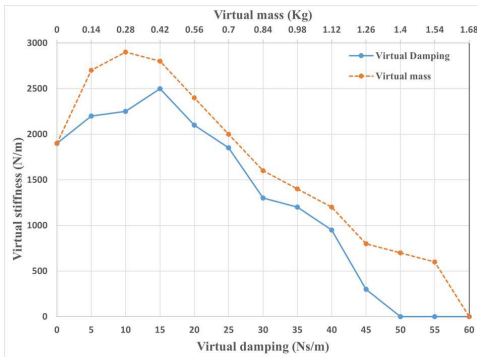


Fig. 5. Z-width plot of HULE for $K_d = 100 \text{ N/m}$ and $B_d = 40 \text{ Ns/m}$ with $t_f = 5 \text{ s}$. The solid line is Z-width with virtual damping and the dashed line is with varying virtual mass. The region under the lines are passive region.

For virtual damping (b_e) varying from 0 to 60 Ns/m with an interval step of 5 Ns/m, and for virtual mass (m_d) varying from 0 to 1.68 kg with an interval of 0.14 kg, the maximum virtual stiffness that can be rendered passively is illustrated in Fig. 5. As can be seen, employing varying virtual mass expands the Z-width of HULE. Moreover, to demonstrate the effect of adding varying virtual mass, in Fig. 6 the result of contact with a virtual wall with $k_e = 2500 \text{ N/m}$ is displayed.

Fig. 6(a) and 6(b) demonstrate that contact without damping element and virtual damping $b_e = 5 \text{ Ns/m}$ is unstable, while with varying virtual mass $m_d = 0.14 \text{ kg}$ passivity condition of (30) is ensured. Considering all the aforementioned along with uncertainties and non-linearities, the Z-width drawn in Fig. 5 is much more reliable and applicable for real-world application.

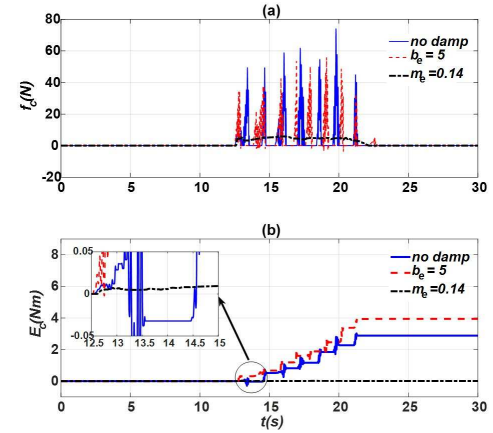


Fig. 6. Contact with the environment with $k_e = 2500 \text{ N/m}$ and $t_f = 5 \text{ s}$, a) contact force plots with and without damping elements, b) energy generation during contact

B. Experimental Results of Designed Controller

The performance of the designed controller is examined in this section. The control goal of HULE is to track a desired square path in $y - z$ plane with the desired orientation while carrying a human arm and having stable contact with a virtual wall with $k_e = 1000 \text{ N/m}$ placed in z direction. Two different paths with t_f of 2 s (fast contact) and 5 s (slow contact) are generated, and the performance of the controller is analyzed. The control parameters are selected as: $\gamma = 10$, $K_{Di} = 0.5$, $K_{Ii} = 7$, $k_{di} = 0.05$, $k_{Ii} = 7$. The HULE robot is the ABLE robot, manufactured by Haption. The control signals are transmitted back and forth to the robot using SIMULINK and Haption interface with a sample time of 1 ms.

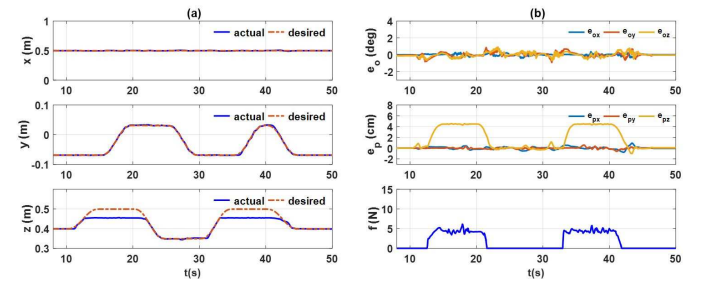


Fig. 7. Experimental results of designed controller with $k_e = 1000 \text{ N/m}$, $m_d = 0.14 \text{ kg}$, and $t_f = 5 \text{ s}$ with contact in z direction. a) position tracking, b) orientation error, position error, and contact force

Fig. 7 demonstrates the performance of the designed control for the 5 s trajectory. Fig. 7(a) shows the tracking of desired trajectory in the $x - y - z$ direction, while Fig. 7(b) shows

the errors of position and orientation tracking along with the contact force. It can be seen that the orientation error is kept at less than 1 deg . Moreover, the position tracking error in the $x - y$ direction is less than 1 cm , while stable contact with the environment is ensured in the z direction. Fig. 8 displays the results for a faster trajectory with t_f of 2 s. It can be concluded from Fig. 8 that although the velocity of the end-effector at the contact point is increased and so does the generated force, the contact is still stable, and the tracking error of position and orientation are less than 1 cm and 2 deg , respectively.

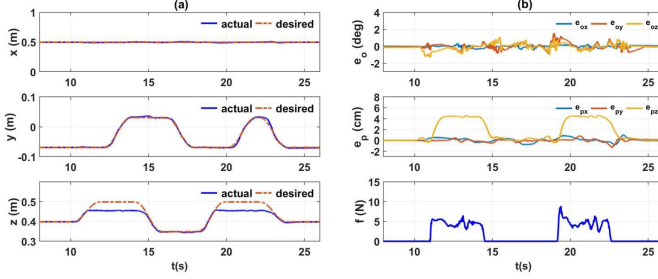


Fig. 8. Experimental results of designed controller with $k_e = 1000 \text{ N/m}$, $m_d = 0.14 \text{ kg}$, and $t_f = 2 \text{ s}$ with contact in z direction. a) position tracking, b) orientation error, position error, and contact force

To show the performance of the controller, the interaction with a virtual wall with $k_e = 1500 \text{ N/m}$ and $t_f = 2 \text{ s}$ is examined in Fig. 9. The stiffness of the environment is increased along with the velocity of the contact, which can result in instability. It can be seen from Fig. 9 that not only is the contact stable, but the controller also shows good performance in keeping tracking errors considerably low.

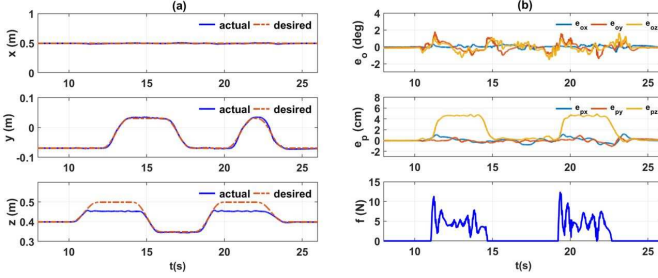


Fig. 9. Experimental results of designed controller with $k_e = 1500 \text{ N/m}$, $m_d = 0.14 \text{ kg}$, and $t_f = 2 \text{ s}$ with contact in z direction. a) position tracking, b) orientation error, position error, and contact force

VII. CONCLUSION

In this study, a subsystem-based adaptive impedance control is designed for the pHREI of a 7-DoF HULE. The designed controller, the so-called VDC scheme, divided the complex system into subsystems consisting of rigid body and actuator dynamics. Then, based on the design variable defined in (26), which is the VDC-impedance law, the required forces and torques are computed in (10) and (14) to track the desired pose of the end-effector during pHREI. Moreover, the adaptation function for estimation of unknown parameters required only one gain for the entire system, yet ensuring the physical consistency condition of estimated parameters. The Z-width

plot of the 7-DoF HULE was drawn, and it was shown that employing varying virtual mass instead of virtual damping can enhance renderable impedances by the haptic display. The experimental results are utilized to analyze the performance of the designed controller. It can be seen from Section VI that HULE with the presented controller perfectly follows the desired path and tolerates human arm and virtual wall forces.

APPENDIX A PROOF FOR THEOREM 2

Substituting (27) and (25) in (26), we have,

$$\begin{aligned} \dot{X}_r &= \dot{X}_d + \Gamma_x(X_d - X) - B_d^{-1}(B_d(\dot{X}_d - \dot{X}) \\ &\quad + K_d(X_d - X)) \\ &= \dot{X}_d + \Gamma_x(X_d - X) - B_d^{-1}B_d(\dot{X}_d - \dot{X}) \\ &\quad - B_d^{-1}K_d(X_d - X) \\ &= \dot{X}_d + \Gamma_x(X_d - X) - \dot{X}_d + \dot{X} - \Gamma_x(X_d - X) \\ &= \dot{X} \end{aligned} \quad (\text{A.1})$$

Now, utilizing result of (A.1) in (26), one can obtain,

$$\begin{aligned} f_d - f &= -\Gamma_f^{-1}(\dot{X}_d - \dot{X}_r) - \Gamma_f^{-1}\Gamma_x(X_d - X) \\ &= -B_d(\dot{X}_d - \dot{X}_r) - K_d(X_d - X) \\ &= -B_d(\dot{X}_d - \dot{X}) - K_d(X_d - X) \end{aligned} \quad (\text{A.2})$$

which shows that the desired impedance in (25) is achieved by robot.

APPENDIX B PROOF FOR THEOREM 3

Subtracting (11) from (9) and (15) from (13) along with using (12) and (16) result in,

$$\begin{aligned} M_{B_i} \frac{d}{dt} {}^{B_i}e_V &= ({}^{B_i}F_r^* - {}^{B_i}F^*) - {}^{B_i}W\tilde{\phi}_{B_i} \\ &\quad - C_{B_i} {}^{B_i}e_V - K_{D_i} {}^{B_i}e_V - K_{I_i} \int_0^t {}^{B_i}e_V dt \end{aligned} \quad (\text{B.1})$$

$$\begin{aligned} I_{mi} \frac{d}{dt} e_{ai} &= (\tau_{ir}^* - \tau_i^*) - W_{ai} \tilde{\phi}_{ai} \\ &\quad - k_{di} e_{ai} - k_{Ii} \int_0^t e_{ai} dt \end{aligned} \quad (\text{B.2})$$

where $\tilde{\phi}_{B_i} = \hat{\phi}_{B_i} - \phi_{B_i}$ and $\tilde{\phi}_{ai} = \hat{\phi}_{ai} - \phi_{ai}$. Taking the time derivative of (28), using Lemma 2, (B.1), (B.2), and conducting mathematical manipulation, we get to,

$$\begin{aligned} \dot{\nu}_i(t) &= \sum_{i=1}^7 [{}^{B_i}e_V^T ({}^{B_i}F_r^* - {}^{B_i}F^*) - \tilde{\phi}_{B_i}^T s_{B_i} \\ &\quad - {}^{B_i}e_V^T K_{D_i} {}^{B_i}e_V + e_{ai} (\tau_{ir}^* - \tau_i^*) - \tilde{\phi}_{ai}^T s_{ai} \\ &\quad - k_{di} e_{ai}^2 + \text{tr}([\hat{\mathcal{L}}_{B_i}^{-1} \dot{\hat{\mathcal{L}}}_{B_i} \hat{\mathcal{L}}_{B_i}^{-1}] \tilde{\mathcal{L}}_{B_i}) \\ &\quad + \text{tr}([\hat{\mathcal{L}}_{ai}^{-1} \dot{\hat{\mathcal{L}}}_{ai} \hat{\mathcal{L}}_{ai}^{-1}] \tilde{\mathcal{L}}_{ai})] \end{aligned} \quad (\text{B.3})$$

with $s_{B_i} = W_{B_i}^T {}^{B_i}e_V$ and $s_{ai} = W_{ai}^T e_{ai}$. By rewriting (B.3) using $\tilde{\phi}_{B_i}^T s_{B_i} = \text{tr}(\tilde{\mathcal{L}}_{B_i} S_{B_i})$ and $\tilde{\phi}_{ai}^T s_{ai} = \text{tr}(\tilde{\mathcal{L}}_{ai} S_{ai})$ where

S_{B_i} and S_{B_i} are unique symmetric matrices, and (17) and (18), we have

$$\begin{aligned}\dot{\nu}_i(t) = & \sum_{i=1}^7 [B_i e_V^T (B_i F_r^* - B_i F^*) + e_{ai} (\tau_{ir}^* - \tau_i^*) \\ & - B_i e_V^T K_{Di} B_i e_V - k_{di} e_{ai}^2].\end{aligned}\quad (\text{B.4})$$

The first two terms on the right side of (B.4) are VPFs related to the rigid body and actuator parts. It can be shown that [23],

$$B_i e_V^T (B_i F_r^* - B_i F^*) = p_{B_i} - p_{T_i} \quad (\text{B.5})$$

$$e_{ai} (\tau_{ir}^* - \tau_i^*) = -p_{B_i} + p_{T_{i-1}} \quad (\text{B.6})$$

where $p_{T_0} = 0$ because the ground has no velocity. By replacing (B.5) and (B.6) in (B.4), it can be concluded that all the VPFs cancel one another at the VCP, except that which represents contact with the environment,

$$\dot{\nu}_i(t) = \sum_{i=1}^7 [-B_i e_V^T K_{Di} B_i e_V - k_{di} e_{ai}^2] - p_{T_7}. \quad (\text{B.7})$$

It is obvious from (B.7) that if p_{T_7} vanishes, the asymptotic stability of the entire system is established.

As the T_7 frame is attached to the end-effector of the robot, its velocity and forces are velocity and forces represented in Cartesian space. Therefore, utilizing the definition of VPF in (16), one can get,

$$\begin{aligned}p_{T_7} &= (T_7 V_r - T_7 V)^T (T_7 F_r - T_7 F) \\ &= (\dot{X}_r - \dot{X})^T (f_d - f)\end{aligned}\quad (\text{B.8})$$

with $T_7 F_r = f_d$. Then, by replacing (25), (26), and (27) in (B.8), we can obtain,

$$\begin{aligned}p_{T_7} &= (\dot{X}_d - \dot{X})^T (B_d B_d^{-1} B_d - B_d) \dot{X}_d - \dot{X} \\ &+ (\dot{X}_d - \dot{X})^T (2B_d^{-1} K_d B_d - K_d - B_d^{-1} K_d B_d) (X_d - X) \\ &+ (X_d - X)^T (K_d B_d^{-1} K_d - K_d B_d^{-1} K_d) (X_d - X) \\ &= 0.\end{aligned}\quad (\text{B.9})$$

Therefore, the time derivative of the accompanying function in (B.7) becomes negative definite, and the stability of the entire system in the sense of Theorem 1 is ensured.

REFERENCES

- R. Jahanmehin, S. Masoud, J. Rickli, and A. Djuric, "Human-robot interactions in manufacturing: A survey of human behavior modeling," *Robotics and Computer-Integrated Manufacturing*, vol. 78, p. 102404, 2022.
- G. Li, Z. Li, and Z. Kan, "Assimilation control of a robotic exoskeleton for physical human-robot interaction," *IEEE Robotics and Automation Letters*, vol. 7, no. 2, pp. 2977–2984, 2022.
- P. Garrec, J.-P. Friconeau, Y. Measson, and Y. Perrot, "Able, an innovative transparent exoskeleton for the upper-limb," in *2008 IEEE/RSJ International Conference on Intelligent Robots and Systems*. IEEE, 2008, pp. 1483–1488.
- N. Hogan, "Impedance control: An approach to manipulation," in *1984 American control conference*. IEEE, 1984, pp. 304–313.
- D. W. Weir, J. E. Colgate, and M. A. Peshkin, "Measuring and increasing z-width with active electrical damping," in *2008 Symposium on Haptic Interfaces for Virtual Environment and Teleoperator Systems*. IEEE, 2008, pp. 169–175.
- E. Shahriari, S. A. B. Birjandi, and S. Haddadin, "Passivity-based adaptive force-impedance control for modular multi-manual object manipulation," *IEEE Robotics and Automation Letters*, vol. 7, no. 2, pp. 2194–2201, 2022.
- Y. Michel, R. Rahal, C. Pacchierotti, P. R. Giordano, and D. Lee, "Bilateral teleoperation with adaptive impedance control for contact tasks," *IEEE Robotics and Automation Letters*, vol. 6, no. 3, pp. 5429–5436, 2021.
- Y. Li, S. S. Ge, and C. Yang, "Impedance control for multi-point human-robot interaction," in *2011 8th Asian Control Conference (ASCC)*. IEEE, 2011, pp. 1187–1192.
- Z. Li, Z. Huang, W. He, and C.-Y. Su, "Adaptive impedance control for an upper limb robotic exoskeleton using biological signals," *IEEE Transactions on Industrial Electronics*, vol. 64, no. 2, pp. 1664–1674, 2016.
- A. M. Khan, D.-w. Yun, M. A. Ali, J. Han, K. Shin, and C. Han, "Adaptive impedance control for upper limb assist exoskeleton," in *2015 IEEE International Conference on Robotics and Automation (ICRA)*. IEEE, 2015, pp. 4359–4366.
- B. Brahmi, M. Driscoll, I. K. El Bojairami, M. Saad, and A. Brahmi, "Novel adaptive impedance control for exoskeleton robot for rehabilitation using a nonlinear time-delay disturbance observer," *ISA transactions*, vol. 108, pp. 381–392, 2021.
- X. Li, Y.-H. Liu, and H. Yu, "Iterative learning impedance control for rehabilitation robots driven by series elastic actuators," *Automatica*, vol. 90, pp. 1–7, 2018.
- M. Sharifi, S. Behzadipour, and G. Vossoughi, "Nonlinear model reference adaptive impedance control for human–robot interactions," *Control Engineering Practice*, vol. 32, pp. 9–27, 2014.
- H. Kim, J. Kwon, Y. Oh, B. J. You, and W. Yang, "Weighted hybrid admittance-impedance control with human intention based stiffness estimation for human-robot interaction," in *2018 IEEE/RSJ International Conference on Intelligent Robots and Systems (IROS)*. IEEE, 2018, pp. 1–6.
- V. Chawda, O. Celik, and M. K. O'Malley, "Application of levant's differentiator for velocity estimation and increased z-width in haptic interfaces," in *2011 IEEE World Haptics Conference*. IEEE, 2011, pp. 403–408.
- K. Lee and D. Y. Lee, "Multirate control of haptic interface for stability and high fidelity," in *2004 IEEE International Conference on Systems, Man and Cybernetics (IEEE Cat. No. 04CH37583)*, vol. 3. IEEE, 2004, pp. 2542–2547.
- M. H. Koul, M. Manivannan, and S. K. Saha, "Enhancing the z-width of haptics interfaces through dual-rate sampling," in *Proceedings of conference on advances in robotics*, 2013, pp. 1–6.
- R. J. Adams and B. Hannaford, "Stable haptic interaction with virtual environments," *IEEE Transactions on robotics and Automation*, vol. 15, no. 3, pp. 465–474, 1999.
- B. Hannaford and J.-H. Ryu, "Time-domain passivity control of haptic interfaces," *IEEE transactions on Robotics and Automation*, vol. 18, no. 1, pp. 1–10, 2002.
- A. R. Tiwari, S. Saha, and S. Kumar, "Improved dual haptic controller with extra virtual damper for z-width enhancement," in *2022 Third International Conference on Intelligent Computing Instrumentation and Control Technologies (ICICICT)*. IEEE, 2022, pp. 78–81.
- H. Choi, N. G. Kim, A. Jafari, H. Singh, and J.-H. Ryu, "Virtual inertia as an energy dissipation element for haptic interfaces," *IEEE Robotics and Automation Letters*, vol. 7, no. 2, pp. 2708–2715, 2022.
- M. Hejrati and J. Mattila, "Decentralized nonlinear control of redundant upper limb exoskeleton with natural adaptation law," in *2022 IEEE-RAS 21st International Conference on Humanoid Robots (Humanoids)*. IEEE, 2022, pp. 269–276.
- W.-H. Zhu, *Virtual decomposition control: toward hyper degrees of freedom robots*. Springer Science & Business Media, 2010, vol. 60.
- S. Lampinen, J. Koivumäki, W.-H. Zhu, and J. Mattila, "Force-sensorless bilateral teleoperation control of dissimilar master–slave system with arbitrary scaling," *IEEE Transactions on Control Systems Technology*, vol. 30, no. 3, pp. 1037–1051, 2021.
- J. Koivumäki and J. Mattila, "Stability-guaranteed impedance control of hydraulic robotic manipulators," *IEEE/ASME Transactions On Mechatronics*, vol. 22, no. 2, pp. 601–612, 2016.
- S. Lampinen, J. Koivumäki, and J. Mattila, "Full-dynamics-based bilateral teleoperation of hydraulic robotic manipulators," in *2018 IEEE 14th International Conference on Automation Science and Engineering (CASE)*. IEEE, 2018, pp. 1343–1350.